

Article pubs.acs.org/JPCA

# Pragmatic Solution for a Fully E,J-Resolved Master Equation

Thanh Lam Nguyen\* and John F. Stanton



Cite This: J. Phys. Chem. A 2020, 124, 2907-2918



**ACCESS** I

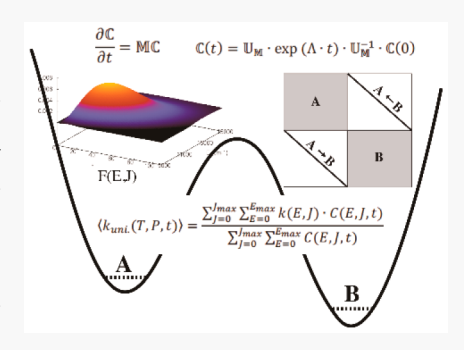
Metrics & More



Article Recommendations

Supporting Information

ABSTRACT: Including the effects of total angular momentum is essential to determine highly accurate pressure-dependent phenomenological rate coefficients when there are significant changes of rotational constants along the reaction coordinate. In this work, a deterministic (matrix) method has been used to solve a completely E,J-resolved twodimensional master equation (2DME) for reaction systems that have many intermediates and many products. The practicality of the method is due to the need to obtain just a few eigenvalues and corresponding eigenvectors. Three examples are provided in order to test the performance of the implementation. It is found that the impact of rotational energy transfer via collisions on a loose transition state (TS) is more noticeable than a tight TS. The calculated results are then compared with those obtained from a recent fixed-J 2DME model.



## ■ INTRODUCTION

In chemical kinetics, a master equation is the name given to a system of coupled integro-differential equations that describes the time evolution of various species in a gas phase reaction, specifically one that includes a complicated competition of unimolecular reactions and weak-collisional energy transfer processes. 1-4 The master equation technique is a powerful tool that is commonly used to compute, predict, and provide rate coefficients—depending on both temperature and pressure for modeling gas-phase reactions occurring in combustion, atmospheric chemistry, and interstellar chemistry. 5-22 For a one-dimensional master equation (1DME) where only (internal) energy transfer is considered in the process, solutions are well documented. 1-4 Such 1DME methods have been implemented into numerous well-known software packages including CHEMRATE, <sup>23</sup> UNIMOL, <sup>24</sup> MES-MER, <sup>25,26</sup> MESS, <sup>27</sup> MULTIWELL, <sup>28</sup> and others; <sup>11,29</sup> some are available free of charge. Nowadays, 1DME methods are routinely used and found to work fairly well for a broad range of reaction systems that have multiple intermediates and multiple products. A second "dimension"—the effects of angular momentum (i.e., centrifugal corrections)—is also sometimes included in 1DME approaches through an indirect approximation 5,6,9,10,22,28 or calculated as an expectation value.30-34 For some reaction pathways where there is a significant change of rotational constants along the reaction coordinate (for example, breaking a single bond C-H of CH<sub>4</sub> to form CH<sub>3</sub> + H), 35 a proper treatment of total angular momentum in computing E,J-resolved microcanonical rate constants as well as in the master equation becomes desirable.

When total angular momentum (J) is included explicitly,36-45 the master equation becomes a two-dimensional (2DME), which fully depends on both total internal energy and total angular momentum quantum number, both of which are allowed to change simultaneously through collisions. 5,7,35,46-48 There are two main issues that prevent the use of a full 2DME approach from becoming routine: one is the need for an E,J-resolved collisional transfer probability distribution function,  $P(E_1,J_1|E_2,J_2)$ ,  $^{38,46,49-52}$  the form of which is practically unknown for most reaction systems; 51-54 the other practical obstacle is the sheer size of the transition matrix, which is too large to permit a routine full diagonalization. As a result, full solutions of the 2DME problem remain rare, at least for reaction systems having multiple wells and multiple product channels.

Jeffrey et al. 46 were the first to report an iterative solution of the 2DME for thermal unimolecular reactions, which have a single well and a single product channel (e.g.,  $C_2H_6 \rightarrow CH_3 +$ CH<sub>3</sub>), using the Nesbet algorithm. <sup>46</sup> To reduce the size of the matrix, and to speed up the calculations, Robertson and coworkers<sup>7,47</sup> then suggested the use of the diffusion equation technique for the vibrational energy space but a discrete treatment for the rotational energy space. The matrix is subsequently simplified to a thin banded one, which is easily handled. It was reported that this technique was about 10 times faster than the Nesbet algorithm.<sup>47</sup> Very recently, Jasper and co-workers<sup>35</sup> have published an excellent paper. These workers have succeeded to predict pressure-dependent rate coefficients for the  $CH_4 \rightarrow CH_3 + H$  and  $C_2H_3 \rightarrow C_2H_2 + H$ reactions from first-principles using an advanced 2DME technique. 5,6,35 In that work, the E,J-resolved collisional

Received: December 8, 2019 Revised: February 24, 2020 Published: March 24, 2020





transfer probabilities were explicitly obtained from classical trajectory calculations, rather than reliance upon an empirical model. The calculated results in that study were found to agree well with experiment. In addition to being impressive, this study is largely unique and can be considered as a triumph of modern chemical kinetics and dynamics. In addition to thermally activated reactions, a 2DME approach for chemically activated reactions was developed by Venkatesh et al. An applied to the association of  $C_2H_5 + O_2$  leading to  $C_2H_4 + HO_2$ .

In previous papers, 30-34 to simplify solution of the 2DME problem, we have proposed the use of the fixed-I approximation where total angular momentum quantum number (1) has been kept unchanged in collisions of a bath gas and an energized molecule. 30-34 On the basis of this assumption, solution of 2DME is reduced to a number of independent 1DMEs, which are relatively straightforward to be solved. This pragmatic model has three important advantages over the usual 1DME approach: (i) the effects of angular momentum are explicitly included in computing microcanonical rate constants k(E,I) (although not in the context of an E,J-resolved collisional transfer probability distribution function  $P(E_1,J|E_2,J) = P(E_1|E_2)_J$ ; pressure-dependent rate constants are then calculated as expectation values; (ii) this fixed-J 2DME model can be applied to any (thermally or chemically activated) reactions having multiple wells and multiple product channels (its range of applicability is the same as that for a 1DME treatment); and (iii) since each particular angular momentum quantum number  $(J_x)$  is completely uncoupled to the other  $J_{v}$ , the fixed-J algorithm is easily done in parallel on any high-performance computing system. It should be mentioned that such a simple (fixed-I) assumption is only exact at the low- and high-pressure limits, but not at moderate pressures, in the falloff regime where a solution of full 2DME is clearly to be preferred.

The purpose of this work is to develop and implement an effective, pragmatic algorithm for a solution of a full 2DME model not only for single well, but also for multiple well reaction systems. A complete *E,J*-resolved 2DME code implementing the ideas here will be incorporated in the MULTIWELL software package<sup>28</sup> in the near future.

# METHODS

An *E,J*-resolved two-dimensional master equation that describes the time evolution of multiple intermediates and multiple products (for example, for the *n*th well) is given by 46,47

$$\frac{\partial C_n(E_i, J_i, t)}{\partial t} = \sum_{J_k=0}^{J_{\text{max}}} \int_{E_k=0}^{E_{\text{max}}} \omega_{LJ} \cdot P(E_i, J_i | E_k, J_k) \cdot C_n(E_k, J_k, t) \cdot dE_k - \omega_{LJ} \cdot C_n(E_i, J_i, t) - \sum_{l \neq n}^{N_{n-l}} k_{n \to l}(E_i, J_i) \cdot C_n(E_i, J_i, t) + \sum_{m \neq n}^{N_{m \to n}} k_{m \to n}(E_i, J_i) \cdot C_m(E_i, J_i, t) + \text{OST}(E_i, J_i)$$
(1)

where  $J_{max}$  is the maximum angular momentum quantum number;  $E_{max}$  is the maximum internal energy;  $C_n(E_iJ_it)$  represents the population density in the nth well of state  $(E_iJ_i)$  and time t;  $\omega_{LJ}$  (in s<sup>-1</sup>) is the Lennard-Jones collisional frequency;  $^{38,56}k_{n\rightarrow l}(E_iJ_i)$  (in s<sup>-1</sup>) is the  $(E_iJ_i)$ -resolved microcanonical rate coefficient from the nth well to the lth

well or to products; and  $P(E_{ij}J_i|E_{kj}J_k)$  is the E,J-resolved collisional transfer probability distribution function from state  $(E_{kj}J_k)$  to state  $(E_{ij}J_i)$ . Details regarding  $P(E_{ij}J_i|E_{kj}J_k)$  are given below.

In considering the 2DME, an important factor is the form of the  $E_JJ$ -resolved collisional transfer probability distribution function  $P(E_1J_1|E_2J_2)$  from an initial state  $(E_2J_2)$  to a final state  $(E_1J_1)$ . Ideally, such data should be obtained from either trajectory calculations  $^{35,49,50,55,57,58}$  or experimental measurements. However, such information is rare. Because of this lack of data, for practical applications, an empirical function is often assumed for the convenience. Here, we assume that the vibrational and rotational energies are uncoupled and can be treated separately. In this case, an  $E_JJ$ -resolved collisional transfer probability distribution function  $P(E_1J_1|E_2J_2)$  can be expressed approximately as a product of the vibrational energy collisional transfer probability distribution function  $P_{\nu}(E_1\nu|E_2\nu)$  and the rotational energy collisional transfer probability distribution function  $P_{\nu}(J_1|J_2)$ :  $^{38,46,60}$ 

$$P(E_1, J_1 | E_2, J_2) = P_{\nu}(E_{1\nu} | E_{2\nu}) \times P_{\nu}(J_1 | J_2)$$
(2)

There are two constraints on the collisional transfer probability distribution function: one is the normalization condition (eq 3), and the other is the detailed balance rule (eq 4).

$$\begin{split} &\sum_{E_{1}=0}^{E_{\max}} \sum_{J_{1}=0}^{J_{\max}} P(E_{1}, J_{1} | E_{2}, J_{2}) = 1 \\ &P_{d}(E_{1}, J_{1} | E_{2}, J_{2}) \times (2J_{2} + 1) \times \rho_{2}(E_{2}, J_{2}) \times \exp\left(-\frac{E_{2}}{RT}\right) \\ &= P_{u}(E_{2}, J_{2} | E_{1}, J_{1}) \times (2J_{1} + 1) \times \rho_{1}(E_{1}, J_{1}) \\ &\times \exp\left(-\frac{E_{1}}{RT}\right), \end{split} \tag{3}$$

where  $P_{\rm d}$  and  $P_{\rm u}$  are the normalized probability distribution functions that correspond to energy transferred (per collision) in downward and upward directions, respectively.

A probability distribution function for energy transferred in a downward direction is given by

$$P_{d}(E_{1}, J_{1}|E_{2}, J_{2}) = P_{d}(E_{\nu_{1}}, J_{1}|E_{\nu_{2}}, J_{2}) = \frac{1}{C(E_{2}, J_{2})}$$

$$\cdot \exp\left(-\frac{E_{\nu_{2}} - E_{\nu_{1}}}{\langle \Delta E_{\nu} \rangle_{d}}\right) \cdot P_{r}(J_{1}|J_{2}) \text{ with } E_{\nu_{2}} \ge E_{\nu_{1}}$$
(5)

Here  $P_r(J_1|J_2)$  is the normalized rotational energy collisional transfer probability distribution function; note that total internal energy is always conserved, and thus,  $E_v + E_r = E_{total}$ . An upward energy transfer probability distribution function is then computed through the condition at detailed balance (eq 4).

In this work, all stationary points are always assumed to be a symmetric top species, of which rotational energy levels are given in Scheme 1.

Here  $E_{2D} = \overline{B}J(J+1)$  is the 2D-rotor, which is assumed to be adiabatic (i.e., total angular momentum is a good quantum number and conserved along the reaction path) and separated from the remaining degrees of freedom. As a result, relative (potential) energies have to be adjusted by this amount of energy accordingly;  $E_{Krot} = (A-\overline{B})K^2$  is the K-rotor, which is

Scheme 1. Rotational Energy Levels of a Symmetric Top Molecule, with  $-J \le K \le +J$  and  $\overline{B} = \sqrt{B \cdot C}$ 

$$E_{rot}(J, K) = \overline{B}J(J+1) + (A-\overline{B})K^2$$

2D-Rotor: Adiabatic K-Rotor: Active

not a good quantum number and assumed to be active; thus, it can be convoluted with the vibrational degrees of freedom. <sup>28</sup> So, the vibrational energy in the paper includes two terms of (active) energy: vibrations and *K*-rotation.

$$G(E, J) = \sum_{K=-J}^{K=+J} G_{\nu}(E - E_{Krot})$$

$$\rho(E, J) = \sum_{K=-J}^{K=+J} \rho_{\nu}(E - E_{Krot})$$
(6)

In eq 5, a single exponential model is assumed for both downward (unnormalized) vibrational and rotational energy collisional transfer probability distribution functions.

$$P_{d_{-\nu}}(E_{\nu_1}|E_{\nu_2}) = \exp\left(-\frac{(E_{\nu_2} - E_{\nu_1})}{\langle \Delta E_{\nu/d}}\right)$$
(7)

with  $E_{\nu 2} \geq E_{\nu 1}$  and  $\langle \Delta E_{\nu} \rangle_d$  is an average vibrational energy transferred in a downward direction.

A downward rotational energy transfer probability distribution function is also given similarly by

$$P_{d_{-r}}(J_1|J_2) = \frac{1}{C_r(J_2)} \cdot e^{-\Delta E_r/\langle \Delta E_r \rangle_d} \text{ with } E_{r2} \ge E_{r1} \text{ or } J_2 \ge J_1$$
(8)

The upward rotational energy transfer is then computed via detailed balance:

$$P_{u_{-r}}(J_2|J_1) \times \rho_{1r}(J_1) \times \exp\left(-\frac{E_{1r}}{RT}\right)$$

$$= P_{d_{-r}}(J_1|J_2) \times \rho_{2r}(J_2) \times \exp\left(-\frac{E_{2r}}{RT}\right)$$
(9)

In eq 8 and eq 9,  $\Delta E_r = E_{r2} - E_{r1}$ ; with  $E_r = BJ(J+1)$ , which is used for the quantum rotational energy level of the 2D-rotor of a symmetric top molecule;  $^{46} \langle \Delta E_r \rangle_d$  is an average rotational energy transferred in a downward direction; and  $C_r(J_2)$  is a normalization factor, which can be computed using a backward substitution method.

In addition to this choice, we have also used another energy transfer function that has been recommended by Jeffrey et al. 46 Both models give relatively the same results; and the difference between the two is negligibly small (see Table S3).

It should be mentioned that the first term on the right-handside of (eq 1) describes the collisional energy transfer rates from other states into state  $(E_{ij}J_i)$ ; the second term defines the collisional energy transfer rates out of state  $(E_{ij}J_i)$  into other states; the third term expresses the population-loss rates from the nth well to other wells or to products; the fourth term represents the population-gain rates from other wells to the nth well; and finally, OST stands for the original source term (it is present only for the first well), which can be omitted for a thermally activated reaction. However, for a chemically activated reaction, it is given by  $1^{-3}$ 

$$OST(E_i, J_i) = F_{CA}(E_i, J_i) \cdot k_{\infty}(T) \cdot [Re_1] \cdot [Re_2]$$
(10)

where  $k_{\infty}(T)$  is the *capture rate constant* of the association step of reactant 1 (Re1) and reactant 2 (Re2) leading to population in well 1, and  $F_{CA}(E_iJ_i)$  is the *E,J*-resolved initial distribution function for the nascent energized well 1, given by<sup>1-3</sup>

$$F_{CA}(E_i, J_i) = \frac{(2J_i + 1) \cdot k_{1 \to Re}(E_i, J_i) \cdot \rho_1(E_i, J_i) \cdot \exp(-E_i/RT)}{\sum_{J_i = 0}^{J_{\max}} (2J_i + 1) \int_{E_i = 0}^{E_{\max}} k_{1 \to Re}(E_i, J_i) \cdot \rho_1(E_i, J_i) \cdot \exp(-E_i/RT) \cdot dE_i}$$
(11)

In eq 11,  $\rho_1(E_{\nu}J_i)$  is the density of rovibrational states for well 1.

For the purpose of practical numerical calculations, the total energy space is divided into small energy bins ("energy grains"), whereby the integrals in eq 1 are converted to sums.

$$\frac{\partial C_n(E_i, J_i, t)}{\partial t} = \sum_{J_k=0}^{J_{\text{max}}} \sum_{E_k=0}^{E_{\text{max}}} \omega_{LJ} \cdot P(E_i, J_i | E_k, J_k) \cdot C_n(E_k, J_k, t) \cdot$$

$$\Delta E - \omega_{LJ} \cdot C_n(E_i, J_i, t) - \sum_{n=1}^{N_{n-1}} k_{n-1}(E_i, J_i) \cdot C_n(E_i, J_i, t)$$

$$+ \sum_{m \neq n}^{N_{m \to n}} k_{m \to n}(E_i, J_i) \cdot C_m(E_i, J_i, t) + OST(E_i, J_i)$$
(12)

Equation 12 can then be cast into the matrix form:

$$\frac{\partial \mathbb{C}}{\partial t} = \mathbb{MC} \tag{13}$$

Here  $\mathbb{C}$  represents the (quite long) vector of population density for all wells, and  $\mathbb{M}$  denotes the transition matrix, which is both vast and sparse; it will be defined below for different reaction systems.

If  $\mathbb M$  can be diagonalized to obtain all eigenvalues  $(\Lambda)$  and corresponding eigenvectors  $(\mathbb U_{\mathbb M})$ , the vector of population density  $(\mathbb C)$  as a function of time can then be expressed as

$$\mathbb{C}(t) = \mathbb{U}_{\mathsf{M}} \cdot \exp(\Lambda \cdot t) \cdot \mathbb{U}_{\mathsf{M}}^{-1} \cdot \mathbb{C}(0)$$
(14)

When  $\mathbb{C}$  is known, flux rate coefficients can be obtained as a function of time:

$$k_{uni.}(T, P, t) = \frac{\sum_{J=0}^{J_{\text{max}}} \sum_{E=0}^{E_{\text{max}}} k(E, J) \cdot C(E, J, t)}{\sum_{J=0}^{J_{\text{max}}} \sum_{E=0}^{E_{\text{max}}} C(E, J, t)}$$
(15)

Product yields are obtained under steady-state conditions (i.e.,  $\frac{\partial C}{\partial t} = 0$ ) while rate constants are set to be equivalent to flux rate coefficients at long times when they become constant (i.e.,  $\frac{\partial k}{\partial t} = 0$ ). <sup>17,18,28</sup>

Note that the matrix  $\mathbb M$  is naturally asymmetric. To facilitate computation, it can be symmetrized to a matrix  $\mathbb B$  before diagonalizing:<sup>4</sup>

$$\mathbb{B} = \mathbb{SMS}^{-1} \tag{16}$$

Here  $\mathbb S$  is a diagonal transformation matrix, which has diagonal elements given by  $^4$ 

$$S(E, J|E, J) = \frac{1}{\sqrt{F_B(E, J)}} \text{ and } S(E, J|, E, J)^{-1} = \sqrt{F_B(E, J)}$$
(17)

where  $F_B$  is the Boltzmann thermal equilibrium distribution function:

$$F_{B}(E,J) = \frac{(2J+1)\cdot\rho(E,J)\cdot\exp\left(-\frac{E}{RT}\right)}{\sum_{J=0}^{J_{\max}}\sum_{E=0}^{E_{\max}}(2J+1)\cdot\rho(E,J)\cdot\exp\left(-\frac{E}{RT}\right)}$$
(18)

This similarity transformation preserves the eigenvalues of  $\mathbb{M}$ , but  $\mathbb{B}$  and  $\mathbb{M}$  have different eigenvectors. The eigenvectors of the original matrix  $\mathbb{M}$  (which is needed) can be obtained simply from those of  $\mathbb{B}$  via the transformation

$$V_{\mathsf{M}} = \mathbb{S}^{-1} V_{\mathsf{B}} \tag{19}$$

Because B is typically very large, computing all eigenvalues and associated eigenfunctions is a daunting task, which effectively sets up the practical limit to the scope of the full 2DME treatment. A simpler, approximate solution can be suggested. It is often observed that there are a few eigenvalues of B—named chemically significant eigenvalues (CSEs) which are well separated by several orders of magnitude from the remaining ones; 5,6,61 these CSEs play the most important role and control chemical kinetics at long times relative to energy relaxation processes, which need not to be at the steady-state condition with respect to chemical changes. Therefore, the 2DME problem can be reduced to computing the CSEs of the matrix B or M. The Bartis-Widom technique, 62 or Miller and Klippenstein's method, 5,6,27,61 may then be used to obtain phenomenological reaction rate coefficients. In this work, ARPACK (a numerical software library for solving large scale eigenvalue problems)<sup>63</sup> is used to calculate CSEs. Whenever possible, LAPACK<sup>64</sup> is also used for cross-checking.

In the following, we give three simple cases where the reaction rate constants can be related directly to one (or two)

 (i) A → P: this reaction has only one well and one product channel; the phenomenological reaction rate coefficient is equivalent to the absolute value of the smallest eigenvalue of the matrix B (or M) (provided that it is well separated from the remaining ones):

$$k(T, P) = |\lambda_1| \tag{20}$$

(ii)  $A \rightarrow P_1$ ,  $P_2$ ,  $P_3$ , ..., and so on: this reaction has only one well, but many products that can be produced from it; the total reaction rate constant, which equals the sum of all individual rate constants leading to each distinctive product, is again equal to the absolute magnitude of the lowest eigenvalue,  $|\lambda_1|$ . To compute each separable rate constant  $(k_{P_i})$ , one must know the corresponding eigenvector  $(C_1)$  of the smallest eigenvalue,  $\lambda_1$ :

$$k_{P_i}(T, P) = \frac{\sum_{J=0}^{J_{\text{max}}} \sum_{E=0}^{E_{\text{max}}} k_{P_i}(E, J) C_1(E, J)}{\sum_{J=0}^{J_{\text{max}}} \sum_{E=0}^{E_{\text{max}}} C_1(E, J)}$$
(21)

(iii)  $A \rightleftharpoons B$ : this is a reversible reaction, which is a closed system in which population density is not lost. Here, the two smallest eigenvalues  $(\lambda_1 \text{ and } \lambda_2)$  control the chemical kinetics of the system. The first eigenvalue  $(\lambda_1)$  is zero; and the second one  $(\lambda_2)$  has a linear relationship to the forward  $(k_f)$  and reverse  $(k_r)$  rate constants:  $^{65,66}$ 

$$k_f + k_r = -\lambda_2 \tag{22a}$$

In addition, when the reaction reaches equilibrium, we have

$$K_{eq} = \frac{k_f}{k_r} \tag{22b}$$

so that the  $k_f$  and  $k_r$  rate constants are given by

$$\begin{split} k_f &= \frac{K_{eq}}{1 + K_{eq}} \cdot |\lambda_2| \\ k_r &= \frac{1}{1 + K_{eq}} \cdot |\lambda_2| \end{split} \tag{22c}$$

Next, we discuss the construction of a relaxation matrix M for a given reaction system. We will consider three common circumstances: one-well, two-well, and three-well systems. On the basis of these templates, generalization to an arbitrary reaction system can be accomplished by straightforward extension.

**For a One-Well Reaction.** Using m bins for the energy space and n bins for angular momentum results in a square matrix  $\mathbb{M}$  having dimension  $(m \cdot n)$ , which is very dense. A proper choice of m and n depends on the particular reaction as well as reaction conditions under consideration. Typically, m is about 1000 (for example, for  $E_{max} = 5 \times 10^4$  cm<sup>-1</sup> with  $\Delta E = 50$  cm<sup>-1</sup>) and n about 20 (for  $J_{max} = 200$  and  $\Delta J = 10$ ). This creates a matrix  $\mathbb{M}$  with dimension  $(2 \times 10^4)$ . In general, the structure of the matrix  $\mathbb{M}$  is

$$\mathsf{M} \equiv \begin{pmatrix} \mathsf{M}_{1,1} & \mathsf{M}_{1,2} & \mathsf{M}_{1,3} & & \mathsf{M}_{1,n-2} & \mathsf{M}_{1,n-1} & \mathsf{M}_{1,n} \\ \mathsf{M}_{2,1} & \mathsf{M}_{2,2} & \mathsf{M}_{2,3} & & \cdots & \mathsf{M}_{2,n-2} & \mathsf{M}_{2,n-1} & \mathsf{M}_{2,n} \\ \mathsf{M}_{3,1} & \mathsf{M}_{3,2} & \mathsf{M}_{3,3} & & \mathsf{M}_{3,n-2} & \mathsf{M}_{3,n-1} & \mathsf{M}_{3,n} \\ \vdots \vdots & & \ddots \ddots & \vdots \vdots \\ \mathsf{M}_{n-2,1} & \mathsf{M}_{n-2,2} & \mathsf{M}_{n-2,3} & & \mathsf{M}_{n-2,n-2} & \mathsf{M}_{n-2,n-1} & \mathsf{M}_{n-2,n} \\ \mathsf{M}_{n-1,1} & \mathsf{M}_{n-1,2} & \mathsf{M}_{n-1,3} & \cdots & & \mathsf{M}_{n-1,n-2} & \mathsf{M}_{n-1,n-1} & \mathsf{M}_{n-1,n} \\ \mathsf{M}_{n,1} & \mathsf{M}_{n,2} & \mathsf{M}_{n,3} & & \mathsf{M}_{n,n-2} & \mathsf{M}_{n,n-1} & \mathsf{M}_{n,n} \end{pmatrix}$$

where the indices refer to certain ranges (bins) of total angular momentum quantum number *J*.

As seen in eq 23, the matrix M comprises  $n^2$  submatrices, each of which has size  $m \times m$  and whose form is detailed below:

For off-diagonal submatrices of the matrix M:

$$\mathbb{M}_{J_{y},J_{x}} = \begin{pmatrix} P(1,J_{y}|1,J_{x}) & P(1,J_{y}|2,J_{x}) & & & P(1,J_{y}|m-1,J_{x}) & P(1,J_{y}|m,J_{x}) \\ P(2,J_{y}|1,J_{x}) & P(2,J_{y}|2,J_{x}) & & & P(2,J_{y}|m-1,J_{x}) & P(2,J_{y}|m,J_{x}) \\ \vdots & & \ddots \ddots & \vdots \\ P(m-1,J_{y}|1,J_{x}) & P(m-1,J_{y}|2,J_{x}) & & & P(m-1,J_{y}|m-1,J_{x}) & P(m-1,J_{y}|m,J_{x}) \\ P(m,J_{y}|1,J_{x}) & P(m,J_{y}|2,J_{x}) & & & P(m,J_{y}|m-1,J_{x}) & P(m,J_{y}|m,J_{x}) \end{pmatrix}$$

$$(24)$$

each element of the small matrix  $M_{J_yJ_x}$  represents an E<sub>J</sub>J-resolved collisional transfer (normalized) probability.

$$M_{J,J} = \begin{pmatrix} A(1|1)_{J} & A(1|2)_{J} & \dots & A(1|m-1)_{J} & A(1|m)_{J} \\ A(2|1)_{J} & A(2|2)_{J} & \dots & A(2|m-1)_{J} & A(2|m)_{J} \\ \vdots & & \ddots & \vdots \\ A(m-1|1)_{J} & A(m-1|2)_{J} & \dots & A(m-1|m-1)_{J} & A(m-1|m)_{J} \\ A(m|1)_{J} & A(m|2)_{J} & \dots & A(m|m-1)_{J} & A(m|m)_{J} \end{pmatrix}$$

$$(25)$$

For submatrices on the diagonal:

Elements in the matrix  $M_{J,J}$  are exactly like those in the 1DME scenario<sup>3</sup> and are given below:

For diagonal elements of the matrix  $M_{I,J}$ :

$$A(i|i)_{J} = -\sum_{l\neq 1}^{N_{l}} k_{1\rightarrow l}(E_{i}, J) - \omega_{LJ} + \omega_{LJ} \cdot P(i, J|i, J)$$

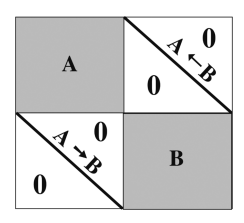
and for off-diagonal elements:

$$A(k|l)_{J} = P(k, J|l, J)$$
(26)

It is worth mentioning that a simplification is achieved when all elements  $P(E_{xy}J_x|E_y,J_y)$  with  $J_x \neq J_y$  are disregarded (i.e., on condition that collisional rotational energy transfer probabilities are negligibly small), all off-diagonal submatrices of the matrix  $\mathbb M$  can be left out. In this case, the solution proposed above reduces exactly to the fixed-J 2DME approach that has been advocated previously.<sup>30–34</sup>

**For a Two-Well Reaction.** The structure of the corresponding matrix M is displayed in Scheme 2:

Scheme 2. Structure of the Transition Matrix  $\ensuremath{\mathbb{M}}$  for a Two-Well Reaction

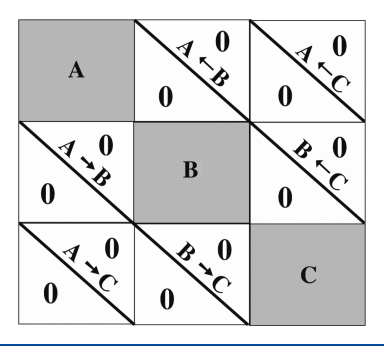


In Scheme 2, the submatrices  $\mathbb{A}$  and  $\mathbb{B}$  have the same composition as the full  $\mathbb{M}$  in the one-well reaction revealed above. Moreover, there are two additional submatrices, which describe the reversible isomerization step of  $A \rightleftarrows B$ . For these two submatrices, all off-diagonal elements are equal to zero; and the diagonal elements represent  $E_JJ$ -resolved micro-

canonical rate constants for the reversible reaction step. As a result of these considerations, the matrix M is both sparse and very large.

For a Three-Well Reaction. Similar to above, the transition matrix M for an arbitrary reaction that has multiple wells is relatively straightforward to construct. For example, with three wells, which can all allow population transfer to any other well, the matrix M is as shown in Scheme 3. Generalization to more complicated scenarios is straightforward, and will quickly lead to matrices of enormous size, underscoring the practical limitations of the 2DME problem.

Scheme 3. Structure of the Transition Matrix  $\mathbb M$  for a Three-Well Reaction



## RESULTS AND DISCUSSION

**Isomerization of CH<sub>3</sub>NC**  $\rightarrow$  **CH<sub>3</sub>CN.** The isomerization of methyl isocyanide (CH<sub>3</sub>NC) to acetonitrile (CH<sub>3</sub>CN) is a textbook reaction, which has been well-characterized experimentally by Rabinovitch and co-workers<sup>67–69</sup> for an extended range of temperature and pressure. Two recent experimental results<sup>70,71</sup> have also agreed well (within 20%) with those published by Rabinovitch. In addition, Rabinovitch et al. also calculated falloff curves using Rice–Ramsperger–Kassel–Marcus (RRKM) theory and a modified model of the strong

collision assumption.<sup>67</sup> The experimental results were consistent with Rabinovitch's theoretical calculations using a collision efficiency factor of 0.6.67 Based on this observation, Rabinovitch et al. concluded that this unimolecular reaction behaves statistically.<sup>67</sup> This is in contrast to results obtained from classical trajectory calculations done by Bunker and Hase, 72,73 who reported nonstatistical behavior (e.g., nonexponential decay) for this reaction. Very recently, Hase and co-workers<sup>74</sup> have restudied this reaction using trajectory calculations based on the density functional theory (DFT) based potential energy surface (PES) and again drawn the same conclusion. This reaction has also recently been investigated using the high accuracy extrapolated ab initio thermochemistry (HEAT) method for the potential energy surface (PES) in combination with Miller's semiclassical transition state theory (SCTST) and the fixed-J 2DME method alluded to the previous section.<sup>33</sup> We have been able to replicate Rabinovitch's falloff curves using either a collision efficiency of 0.7 with the modified strong collision model or an average down energy transferred per collision of ca. 2500 cm<sup>-1</sup> with the fixed-J 2DME approach.<sup>33</sup> The latter value seems to be unusually large, suggesting that its unphysical value is somehow absorbing into the parameter space the effects of the nonstatistical behavior noted by Hase et al. 74 At the highpressure limit where the Boltzmann thermal energy distribution is established, rate constants calculated with the HEAT/ SCTST approach from first-principles (without any adjusted parameters) agree well with those of experiments within

Here, we investigate the effects of angular momentum transfer by collisions on the calculated rate constants in the falloff regime through a full solution of the 2DME. It should be noted that, for this scenario, numerical computations with high-precision floating-point formats (greater than doubleprecision) must be applied for two reasons: (i) first, the rate constant calculated at the high-pressure limit  $(9.8 \times 10^{-4} \text{ s}^{-1})$  at  $P = 10^5$  Torr and T = 504 K) is about  $10^{15}$  smaller than a collision frequency  $(1.16 \times 10^{12} \text{ s}^{-1})$ ; (ii) second, the ratio of the largest and smallest eigenvalues (obtained by diagonalizing the matrix M) is on the of order 10<sup>15</sup>, which is the effective upper limit of a double-precision floating-point calculation. This makes the smallest eigenvalue, which corresponds to the reaction rate constant, numerically unreliable. In this work, quadruple-precision floating-point arithmetic—which provides 33 significant digits of precision—is utilized although it has a significant and negative impact on computation time. It should be mentioned that unstable numerical results were previously reported and discussed.<sup>22</sup> Alternative solutions to this problem were proposed.<sup>3,9,10,25,26</sup>

The potential energy surface, rovibrational parameters and anharmonic constants were reported elsewhere are reused here. The same and an animonic constants were reported elsewhere are reused here. The same are surfaced here, and so on are given in Table 1, from which a transition matrix M having dimensions of 11,713 is constructed. This data set is selected to ensure that the calculated results are converged to within 2% under the conditions considered here. It takes about 5 h of computer time on a computer with 128GB, which is part of the HiPerGator system at the University of Florida, to obtain a few small eigenvalues using ARPACK. The smallest eigenvalues calculated at T = 503.6 K as functions of pressure and average rotational energy transferred per collision in a downward

Table 1. Collisional Parameters Used in the *E,J*-Resolved 2DME Model

parameters	values	
C <sub>2</sub> H <sub>6</sub> : bath gas	mass = 30 g/mol, $\sigma$ = 4.39 Å, $\varepsilon/k_B$ = 234 K <sup>a</sup>	
CH <sub>3</sub> NC/CH <sub>3</sub> CN	mass = 42 g/mol, $\sigma$ = 4.47 Å, $\varepsilon/k_B$ = 380 K <sup>b</sup>	
$E_{ m max}$	27,000 cm <sup>-1</sup> above CH <sub>3</sub> NC	
$\Delta E$ = energy grain	$30 \text{ cm}^{-1}$	
$\langle \Delta E_{ m vib}  angle_{ m d}$	2500 cm <sup>-1</sup>	
$J_{\max}$	120	
$\Delta J$	10	
<sup>a</sup> From Hippler et al. <sup>59</sup> <sup>b</sup> From Fletcher et al. <sup>68</sup>		

direction are displayed in Table 2. The relative difference (as defined in eq 27 below) between a solution of full 2DME and that of the fixed-J 2DME approach is plotted in Figure 1. The relative difference clearly decreases with increasing pressure and with reducing  $\langle \Delta E_{rot} \rangle_d$  as expected. Results obtained with the two methods converge at the high-pressure limit where the reaction rate constant becomes completely independent of the individual value of  $\langle \Delta E_{rot} \rangle_d$  used. Figure 1 also shows the difference found at the lower pressure; at P = 0.01 Torr (the lowest pressure considered here and done in the experiment), the largest difference is found to be about 6% only using a (preposterously unphysical) value  $\langle \Delta E_{rot} \rangle_d$  of 4000 cm<sup>-1</sup>. These results suggest that the fixed-J 2DME is a good approximation for a (very) tight transition state (TS), as in this scenario. This finding is important because the fixed-J 2DME calculations are much cheaper to do and can moreover be applied to arbitrary reaction systems. In addition, in most practical applications such as in atmospheric and combustion environments, the pressures under consideration are much higher (at least 100 Torr), and the fixed-J 2DME approach becomes more accurate. It is worth emphasizing that, as  $\langle \Delta E_{rot} \rangle_d$  approaches to zero, the full 2DME becomes equivalent to the fixed-J 2DME (see eq 28).

relative difference(%) = 
$$\frac{\lambda_{full\_2DME} - \lambda_{fixed\_J}}{\lambda_{fixed\_J}} \times 100\%$$
(27)

$$\lim_{\langle \Delta E_{rot} \rangle_d \to 0} \lambda_{full\_2DME} = \lambda_{fixed\_J}$$
(28)

**Pyrolysis of NH**<sub>3</sub>  $\rightarrow$  **NH**<sub>2</sub> + **H.** Ammonia (NH<sub>3</sub>) is a ubiquitous compound that has also been well-known as an additional chemical component of fuel for many years; <sup>75</sup> it can be added to depress NO<sub>x</sub> emission in internal combustion engines as well as to convert NO<sub>x</sub> pollutants to N<sub>2</sub> in the presence of a proper catalyst. <sup>76</sup> NH<sub>3</sub> has also been manufactured in massive quantities through Haber process, mostly for making fertilizers for agriculture. In recent years, NH<sub>3</sub> has gained some considerations as a promising alternative fuel source that is both renewable and carbon-free. <sup>77–79</sup>

The thermal dissociation of  $\mathrm{NH_3}$  to  $\mathrm{NH_2}$  + H is barrierless and proceeds via a very loose (variational) TS, and there are substantial changes in rotational constants along the reaction coordinate. Therefore, the effects of total angular momentum quantum number on the calculated rate constants in the falloff regime cannot be ignored. This has been seen in a recent study where the calculated rate constants are found to depend sensitively on the specific master-equation model used to treat total angular momentum. There, it was found that the experimental results lie between those found with fixed-J

Table 2. Unimolecular Rate Constant (in s<sup>-1</sup>) for the Isomerization of CH<sub>3</sub>NC  $\rightarrow$  CH<sub>3</sub>CN Calculated as Functions of Pressure (in Torr) and Average Rotational Energy Transferred (in cm<sup>-1</sup>) in a Downward Direction,  $\langle \Delta E_{rot} \rangle_d^a$ 

$\begin{array}{c ccccccccccccccccccccccccccccccccccc$	$\langle \Delta E_{\text{rot}} \rangle_{\text{d}} = 2500$ $8.411 \times 10^{-7}$ $2.102 \times 10^{-6}$ $3.216 \times 10^{-6}$	$\langle \Delta E_{\rm rot} \rangle_{\rm d} = 4000$ $8.417 \times 10^{-7}$ $2.104 \times 10^{-6}$
$\begin{array}{cccccccccccccccccccccccccccccccccccc$	$2.102 \times 10^{-6}$	
$\begin{array}{cccccccccccccccccccccccccccccccccccc$		$2.104 \times 10^{-6}$
$\begin{array}{cccccccccccccccccccccccccccccccccccc$	3 216 🗸 10 🖰	_6
$\begin{array}{cccccccccccccccccccccccccccccccccccc$		$3.218 \times 10^{-6}$
$\begin{array}{cccccccccccccccccccccccccccccccccccc$	$4.253 \times 10^{-6}$	$4.256 \times 10^{-6}$
$\begin{array}{cccccccccccccccccccccccccccccccccccc$	$5.716 \times 10^{-6}$	$5.720 \times 10^{-6}$
$\begin{array}{cccccccccccccccccccccccccccccccccccc$	$1.412 \times 10^{-5}$	$1.412 \times 10^{-5}$
$\begin{array}{cccccccccccccccccccccccccccccccccccc$	$2.137 \times 10^{-5}$	$2.138 \times 10^{-5}$
$\begin{array}{cccccccccccccccccccccccccccccccccccc$	$2.798 \times 10^{-5}$	$2.800 \times 10^{-5}$
$\begin{array}{cccccccccccccccccccccccccccccccccccc$	$3.711 \times 10^{-5}$	$3.714 \times 10^{-5}$
$\begin{array}{cccccccccccccccccccccccccccccccccccc$	$8.542 \times 10^{-5}$	$8.547 \times 10^{-5}$
$\begin{array}{cccccccccccccccccccccccccccccccccccc$	$1.225 \times 10^{-4}$	$1.226 \times 10^{-4}$
30 $3.378 \times 10^{-4}$ $3.453 \times 10^{-4}$ $3.486 \times 10^{-4}$ $3.504 \times 10^{-4}$ $3.510 \times 10^{-4}$ 50 $4.254 \times 10^{-4}$ $4.337 \times 10^{-4}$ $4.373 \times 10^{-4}$ $4.393 \times 10^{-4}$ $4.399 \times 10^{-4}$	$1.535 \times 10^{-4}$	$1.536 \times 10^{-4}$
50 $4.254 \times 10^{-4}$ $4.337 \times 10^{-4}$ $4.373 \times 10^{-4}$ $4.393 \times 10^{-4}$ $4.399 \times 10^{-4}$	$1.925 \times 10^{-4}$	$1.926 \times 10^{-4}$
	$3.514 \times 10^{-4}$	$3.515 \times 10^{-4}$
	$4.403 \times 10^{-4}$	$4.405 \times 10^{-4}$
70 $4.857 \times 10^{-4}$ $4.942 \times 10^{-4}$ $4.980 \times 10^{-4}$ $5.001 \times 10^{-4}$ $5.007 \times 10^{-4}$	$5.011 \times 10^{-4}$	$5.013 \times 10^{-4}$
100 $5.499 \times 10^{-4}$ $5.584 \times 10^{-4}$ $5.622 \times 10^{-4}$ $5.643 \times 10^{-4}$ $5.649 \times 10^{-4}$	$5.653 \times 10^{-4}$	$5.655 \times 10^{-4}$
300 $7.302 \times 10^{-4}$ $7.373 \times 10^{-4}$ $7.405 \times 10^{-4}$ $7.422 \times 10^{-4}$ $7.428 \times 10^{-4}$	$7.431 \times 10^{-4}$	$7.433 \times 10^{-4}$
500 $7.974 \times 10^{-4}$ $8.033 \times 10^{-4}$ $8.059 \times 10^{-4}$ $8.074 \times 10^{-4}$ $8.078 \times 10^{-4}$	$8.081 \times 10^{-4}$	$8.083 \times 10^{-4}$
700 $8.344 \times 10^{-4}$ $8.395 \times 10^{-4}$ $8.418 \times 10^{-4}$ $8.430 \times 10^{-4}$ $8.434 \times 10^{-4}$	$8.437 \times 10^{-4}$	$8.438 \times 10^{-4}$
1000 $8.674 \times 10^{-4}$ $8.717 \times 10^{-4}$ $8.736 \times 10^{-4}$ $8.746 \times 10^{-4}$ $8.749 \times 10^{-4}$	$8.751 \times 10^{-4}$	$8.753 \times 10^{-4}$
3000 $9.339 \times 10^{-4}$ $9.359 \times 10^{-4}$ $9.369 \times 10^{-4}$ $9.374 \times 10^{-4}$ $9.375 \times 10^{-4}$	$9.376 \times 10^{-4}$	$9.377 \times 10^{-4}$
5000 $9.509 \times 10^{-4}$ $9.523 \times 10^{-4}$ $9.529 \times 10^{-4}$ $9.532 \times 10^{-4}$ $9.533 \times 10^{-4}$	$9.534 \times 10^{-4}$	$9.534 \times 10^{-4}$
7000 9.588 $\times$ 10 <sup>-4</sup> 9.598 $\times$ 10 <sup>-4</sup> 9.603 $\times$ 10 <sup>-4</sup> 9.605 $\times$ 10 <sup>-4</sup> 9.606 $\times$ 10 <sup>-4</sup>	$9.607 \times 10^{-4}$	$9.607 \times 10^{-4}$
10000 $9.650 \times 10^{-4}$ $9.658 \times 10^{-4}$ $9.661 \times 10^{-4}$ $9.663 \times 10^{-4}$ $9.663 \times 10^{-4}$	$9.664 \times 10^{-4}$	$9.664 \times 10^{-4}$
30000 $9.753 \times 10^{-4}$ $9.755 \times 10^{-4}$ $9.757 \times 10^{-4}$ $9.757 \times 10^{-4}$ $9.758 \times 10^{-4}$	$9.758 \times 10^{-4}$	$9.758 \times 10^{-4}$
50000 $9.774 \times 10^{-4}$ $9.776 \times 10^{-4}$ $9.777 \times 10^{-4}$ $9.777 \times 10^{-4}$ $9.777 \times 10^{-4}$	$9.777 \times 10^{-4}$	$9.777 \times 10^{-4}$
70000 $9.784 \times 10^{-4}$ $9.785 \times 10^{-4}$ $9.785 \times 10^{-4}$ $9.786 \times 10^{-4}$ $9.786 \times 10^{-4}$		
100000 $9.791 \times 10^{-4}$ $9.792 \times 10^{-4}$ $9.792 \times 10^{-4}$ $9.792 \times 10^{-4}$ $9.792 \times 10^{-4}$	$9.786 \times 10^{-4}$	$9.786 \times 10^{-4}$

<sup>&</sup>lt;sup>a</sup>The rate constants below appear to be converged to about 1–2% (see the Supporting Information).

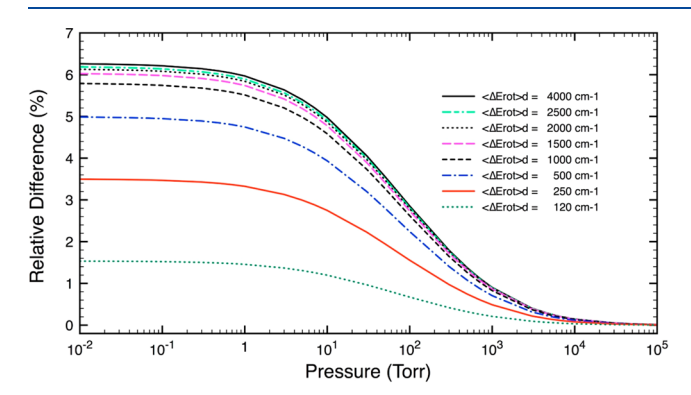


**Figure 1.** Relative difference (%) of full solutions of 2DME and the fixed-J 2DME for the CH<sub>3</sub>NC  $\rightarrow$  CH<sub>3</sub>CN isomerization calculated at T=503.6 K as functions of pressure and average rotational energy transferred per collision in a downward direction,  $\langle \Delta E_{rot} \rangle_d$ . Note that the fixed-J method is accurate to within 7% under all conditions.

2DME and fixed-*J*,*K* 3DME models.<sup>80</sup> Here, this reaction is investigated using a full solution of 2DME, and the calculated results are compared with those of the fixed-*J* 2DME model. All energies, rovibrational parameters, and collisional parameters reported previously<sup>80</sup> are adopted here for the 2DME simulation. The calculated phenomenological rate constants at  $T=1800~\rm K$  as functions of pressure and  $\langle \Delta E_{rot} \rangle_d$  are given in Table S1 (see the Supporting Information), and the relative differences of solutions of full 2DME and the fixed-*J* 2DME are

displayed in Figure 2. Inspection of the latter shows that the relative difference again decreases marginally with increasing

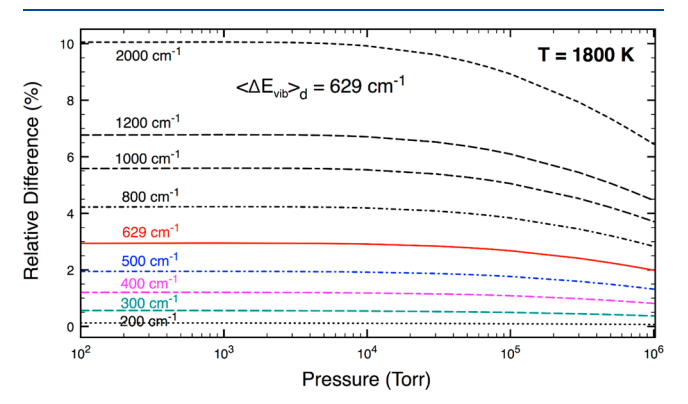


**Figure 2.** Relative difference (%) of solutions of full 2DME and the fixed-J 2DME for the pyrolysis of NH<sub>3</sub> calculated at  $T=1800~{\rm K}$  as functions of pressure and average rotational energy transferred per collision in a downward direction,  $\langle \Delta E_{rot} \rangle_d$ .

pressure, and it rises slightly from about near 0% to 10% when  $\langle \Delta E_{rot} \rangle_d$  is enlarged from 200 to 2000 cm $^{-1}$ . Note that  $\langle \Delta E_{rot} \rangle_d$  = 2000 cm $^{-1}$  is again unphysically large, but might be presumed in a strong-collisional model for rotational energy transfer. Classical mechanics trajectory calculations can, in principle, provide both quantities of  $\langle \Delta E_{vib} \rangle_d$  and  $\langle \Delta E_{rot} \rangle_d$ , but such information is very rare in practice.

an average (internal) energy (which should include both vibrational and rotational energies) transferred per collision is sometimes measured. SP Because of the dearth of data at hand, it is plausible here to assume that  $\langle \Delta E_{rot} \rangle_d$  may be equivalent to  $\langle \Delta E_{vib} \rangle_d$  which is 629 cm<sup>-1</sup> (at T=1800 K, see Table S2) in our calculations. Overall, as seen in Figure 2, the effects of the change of rotational energy by collisions on the phenomenological rate constant are found to be rather weak, well under 10% in this example. If the weak-collisional model is also assumed for rotational energy transfer here, such effects become negligible. This finding is likely to imply that the fixed-J 2DME approach is a very good approximation for the pyrolysis of NH<sub>3</sub>.

Thermal Dissociation of Criegee syn-CH<sub>3</sub>CHOO → CH<sub>2</sub>CHO + OH. Criegee intermediates are very reactive species produced by the ozonolysis of olefins. Although the mechanism for Criegee formation was proposed in 1931,81,82 those molecules have been detected experimentally only very recently. 83-89 It is widely accepted that Criegee intermediates play important roles in producing OH radicals and lowvolatility organic compounds in the atmosphere. 90 Under atmospheric conditions, the ozonolysis of olefins can yield both vibrationally excited (hot) and collisionally thermalized (cool) Criegees,<sup>31</sup> but their fates are very different. A hot Criegee has sufficient energy to rapidly undergo a further decomposition to yield OH. A cool Criegee has a longer lifetime, thus surviving in the air for a while, with a fate depending on its chemical structure as well as the environment in which it is produced. It is believed that the lifetime of a cool Criegee intermediate in the atmosphere is mainly determined through its thermal unimolecular dissociation rate<sup>32,91</sup> or its reaction with water vapor.8

In a previous paper, we reported falloff curves for the Criegee acetaldehyde oxide, syn-CH3CHOO, based on the mHEAT-345(Q) PES and the fixed-J 2DME calculations.<sup>32</sup> At the generic conditions of T = 298 K and P = 1 atm that is (in this scenario) almost close to the high-pressure limit, the predicted rate constant (124 s<sup>-1</sup>)<sup>32</sup> is in good agreement with an experimental estimate 92 and with other theoretical results. 93-95 As compared to other possible removal paths, the thermal unimolecular dissociation of Criegee syn-CH3CHOO was found to predominate at atmospheric conditions.<sup>32</sup> In this work, the thermal dissociation of syn-CH<sub>3</sub>CHOO is studied using a full solution of 2DME to evaluate the sensitivity of the falloff curve to the rotational energy transfer via collisions. All data, including energies, rovibrational parameters, anharmonic constants, and collisional parameters published previously,<sup>32</sup> will be reused here in the 2DME simulation.

Figure 3 displays a schematic reaction energy profile of the decomposition of Criegee syn-CH<sub>3</sub>CHOO (SYN) calculated at the mHEAT-345(Q) level of theory. It first isomerizes via a very tight TS1 leading to hot vinyl hydroperoxide (VHP\*); next, VHP\* decomposes rapidly via a fairly loose TS2 to a van der Waals complex (vdW); finally, vdW yields OH + CH<sub>2</sub>CHO in an effectively spontaneous fashion. This is the major pathway, which is also known as a "well-skipping" mechanism (via highly vibrationally excited VHP\*) and contributes more than 95% at 298 K and 1 atm. The remaining fraction (<5%) is for a thermalized stabilization of VHP through colliding with the bath gas. The ultimate fate of thermalized VHP seems to be a thermal unimolecular decay, thus ending up with the same products OH + CH<sub>2</sub>CHO, but

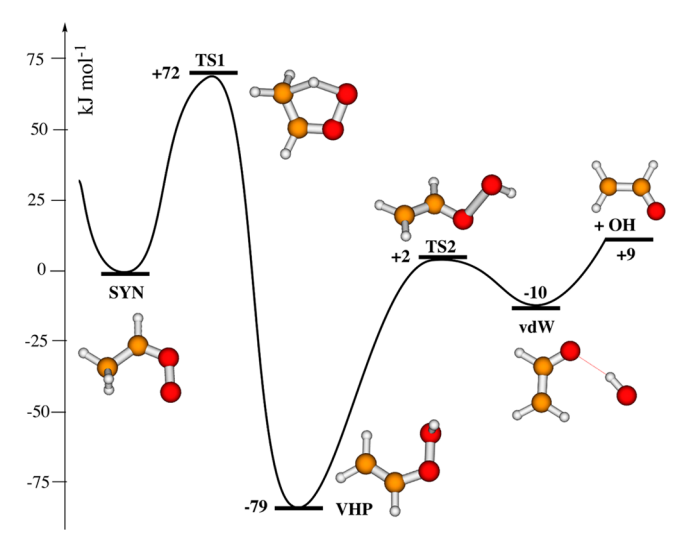


**Figure 3.** Schematic reaction energy profile for the thermal unimolecular dissociation of Criegee syn-CH<sub>3</sub>CHOO  $\rightarrow$  OH + CH<sub>2</sub>CHO calculated at the mHEAT-345(Q) method.

this secondary chemistry mechanism takes a longer time.<sup>32</sup> In the following ME simulation, both **SYN** and **VHP** (i.e., two-well reaction system) are included, but not **vdW**. This simplification leads to a slight overestimate of the thermal rate constant of **VHP**, but does not impact the well-skipping pathway via TS1, which is kinetically governing in this case. It should be mentioned that both the tight TS1 and the loose TS2 are included in the 2DME simulation, thus allowing us to see these interesting joint effects on the falloff curve.

In this two-well reaction system, there are two important, smallest eigenvalues ( $\lambda_1$  and  $\lambda_2$ ) that are well-separated from the remaining ones by more than 5 orders of magnitude. The phenomenological rate coefficients can be derived using these two chemically significant eigenvalues. As shown elsewhere, <sup>32</sup> the smallest eigenvalue  $|\lambda_1|$  is directly equivalent to the dissociation rate constant of VHP while the second smallest one  $|\lambda_2|$  is equal to the total dissociation rate constant of SYN. Therefore, here we study the effects of the change of total angular momentum through collisions on both  $\lambda_1$  and  $\lambda_2$ . Figures 4 and 5 show such impacts as functions of pressure and  $\langle \Delta E_{rot} \rangle_d$ . Overall, these two figures look qualitatively similar to Figures 1 and 2. They exhibit similar trends in that the relative

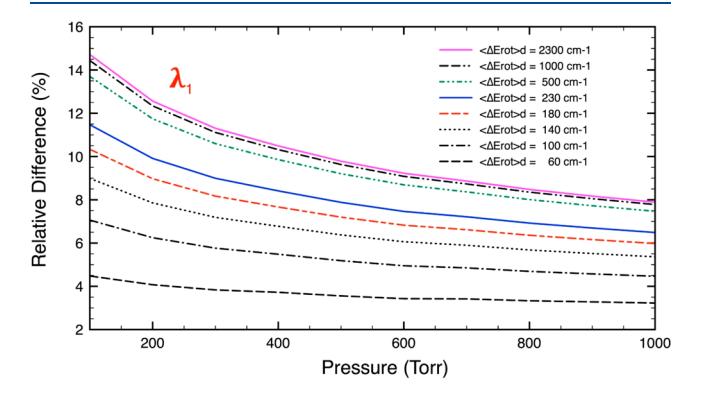
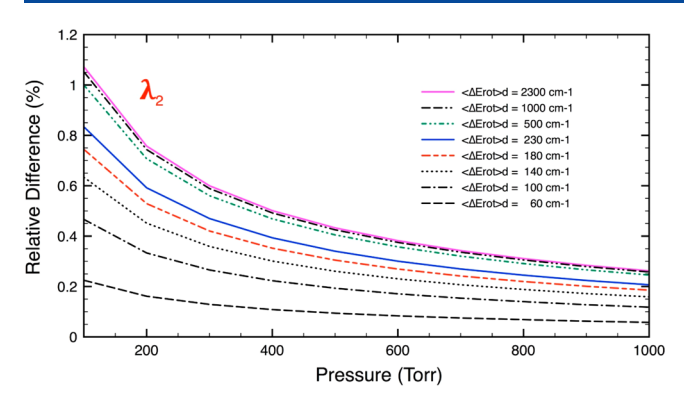


Figure 4. Relative difference (%) of the  $E_J$ -resolved 2DME and the fixed-J 2DME for  $\lambda_1$  from the thermal dissociation of syn-CH<sub>3</sub>CHOO calculated at T=300 K as functions of pressure and average rotational energy transferred per collision in a downward direction,  $\langle \Delta E_{rot} \rangle_d$ .



**Figure 5.** Relative difference (%) of the *E,J*-resolved 2DME and the fixed-*J* 2DME for  $\lambda_2$  from the thermal dissociation of syn-CH<sub>3</sub>CHOO calculated at T = 300 K as functions of pressure and average rotational energy transferred per collision in a downward direction,  $\langle \Delta E_{rot} \rangle_d$ .

difference slightly decreases as pressure increases; and it increases with the larger value of  $\langle \Delta E_{rot} \rangle_d$ . Interestingly (but it can be expected), the effect on  $\lambda_1$  is more pronounced because TS2 is fairly loose; in contrast, the influence on  $\lambda_2$  is virtually insignificant because TS1 is very tight.

For this scenario, passing over (or through by tunneling) TS1 (associated with  $\lambda_2$ ) is the rate-determining step. Therefore, the fixed-J 2DME results remain highly accurate because they agree closely (within 1%) to the fully *E,J*-resolved 2DME (see Figure 5). To the best of our knowledge, this is the first time a full solution of 2DME for a two-well reaction system has been determined. It is desirable to apply this method to other (complicated) reaction systems, and efforts in that direction are planned.

## CONCLUSIONS

Iterative solutions of E,J-resolved 2DME problem for some reaction systems comprising one well and one product were formerly reported in the literature. 35,46,47 In this work, we have developed and implemented a pragmatic solution of completely E,J-resolved 2DME applicable to multiple well and multiple channel reactions. Three reactions that have different characteristics are used to test the performance of the new implementation. As compared to the fixed-J 2DME model, the E,J-resolved 2DME approach gives slightly higher phenomenological rate coefficients although the differences are less than 15% in all cases studied. However, this does not ensure that such a small difference can also be expected for other reactions. A further test for an extended reaction system is certainly warranted. In addition, effects of the rotational energy transfer through collisions on a loose TS are found to be more pronounced than a tight TS. Given that the fully E,Jresolved 2DME calculations are very expensive, the fixed-J 2DME model-which is now calibrated-is an effective compromise and a practical tool. However, the fully E,Jresolved 2DME calculations may be desired for benchmarking high-accuracy rate constants. Efficient iterative methods in searching for chemically significant eigenvalues, in combination with fast parallel algorithms on high-performance computer systems, can be used to speed up the solutions of the E,Jresolved 2DME problem.

## ASSOCIATED CONTENT

## Supporting Information

The Supporting Information is available free of charge at https://pubs.acs.org/doi/10.1021/acs.jpca.9b11379.

Collisional parameters, the calculated rate coefficients, and additional figures are provided (PDF)

#### AUTHOR INFORMATION

## **Corresponding Author**

Thanh Lam Nguyen — Quantum Theory Project, Departments of Chemistry and Physics, University of Florida, Gainesville, Florida 32611, United States; ⊚ orcid.org/0000-0002-7794-9439; Email: tlam.nguyen@chem.ufl.edu

#### **Author**

John F. Stanton — Quantum Theory Project, Departments of Chemistry and Physics, University of Florida, Gainesville, Florida 32611, United States; orcid.org/0000-0003-2345-9781

Complete contact information is available at: https://pubs.acs.org/10.1021/acs.jpca.9b11379

#### Notes

The authors declare no competing financial interest.

## ACKNOWLEDGMENTS

This material is based on work supported by the U.S. Department of Energy, Office of Basic Energy Sciences under Award DE-FG02-07ER15884 and the U.S. Air Force Office of Scientific Research (No. FA9550-16-1-0117). Aspects of this work were also supported by the U.S. National Science Foundation, under Grant CHE-1748821. We would like to thank Prof. John R. Barker, Dr. Struan H. Robertson, and Dr. György Lendway for sharing their excellent review articles. We would also like to express our gratitude to two anonymous reviewers for their useful comments that improved the quality of this paper.

# REFERENCES

- (1) Robinson, P. J.; Holbrook, K. A. *Unimolecular reactions*; Wiley-Interscience: London and New York, 1972.
- (2) Forst, W. Theory of unimolecular reactions. Academic Press: New York, 1973.
- (3) Holbrook, K. A.; Pilling, M. J.; Robertson, S. H.; Robinson, P. J. *Unimolecular reactions*, 2nd ed.; Wiley: Chichester, U.K. and New York, 1996.
- (4) Gilbert, R. G.; Smith, S. C. Theory of unimolecular and recombination reactions; Blackwell Scientific Publications: Oxford, U.K., and Boston, MA, 1990.
- (5) Miller, J. A.; Klippenstein, S. J.; Raffy, C. Solution of Some Oneand Two-Dimensional Master Equation Models for Thermal Dissociation: The Dissociation of Methane in the Low-Pressure Limit. J. Phys. Chem. A 2002, 106, 4904—4913.
- (6) Miller, J. A.; Klippenstein, S. J. Master equation methods in gas phase chemical kinetics. *J. Phys. Chem. A* **2006**, *110* (36), 10528–44.
- (7) Robertson, S. H.; Pilling, M. J.; Green, N. J. B. Diffusion approximations of the two-dimensional master equation. *Mol. Phys.* **1996**, 89 (5), 1531–1551.
- (8) Pilling, M. J.; Robertson, S. H. Master equation models for chemical reactions of importance in combustion. *Annu. Rev. Phys. Chem.* **2003**, *54*, 245–75.
- (9) Frankcombe, T. J.; Smith, S. C. Time evolution in the unimolecular master equation at low temperatures: full spectral

- solution with scalable iterative methods and high precision. *Comput. Phys. Commun.* **2001**, *141* (1), 39–54.
- (10) Frankcombe, T. J.; Smith, S. C.; Gates, K. E.; Robertson, S. H. A master equation model for bimolecular reaction via multi-well isomerizing intermediates. *Phys. Chem. Chem. Phys.* **2000**, *2*, 793–803.
- (11) Vereecken, L.; Huyberechts, G.; Peeters, J. Stochastic simulation of chemically activated unimolecular reactions. *J. Chem. Phys.* **1997**, *106* (16), 6564–6573.
- (12) Vereecken, L.; Peeters, J. Detailed microvariational RRKM master equation analysis of the product distribution of the  $C_2H_2+CH(X^2Pi)$  reaction over extended temperature and pressure ranges. J. Phys. Chem. A 1999, 103 (28), 5523–5533.
- (13) Zhang, J.; Donahue, N. M. Constraining the mechanism and kinetics of OH + NO<sub>2</sub> and HO<sub>2</sub> + NO using the multiple-well master equation. *J. Phys. Chem. A* **2006**, *110* (21), 6898–911.
- (14) Barker, J. R. Monte-Carlo Calculations on Unimolecular Reactions, Energy-Transfer, and IR-Multiphoton Decomposition. *Chem. Phys.* **1983**, 77 (2), 301–318.
- (15) Barker, J. R. Multiple-well, multiple-path unimolecular reaction systems. I. MultiWell computer program suite. *Int. J. Chem. Kinet.* **2001**, 33 (4), 232–245.
- (16) Olzmann, M.; Kraka, E.; Cremer, D.; Gutbrod, R.; Andersson, S. Energetics, kinetics, and product distributions of the reactions of ozone with ethene and 2,3-dimethyl-2-butene. *J. Phys. Chem. A* **1997**, 101 (49), 9421–9429.
- (17) Bedanov, V. M.; Tsang, W.; Zachariah, M. R. Master equation analysis of thermal-activation reactions-reversible isomerization and decomposition. *J. Phys. Chem.* **1995**, *99* (29), 11452–11457.
- (18) Tsang, W.; Bedanov, V.; Zachariah, M. R. Master equation analysis of thermal activation reactions: Energy-transfer constraints on falloff behavior in the decomposition of reactive intermediates with low thresholds. *J. Phys. Chem.* **1996**, *100* (10), 4011–4018.
- (19) Green, N. J. B. Steady-state master equation methods. Unimolecular Kinetics: Parts 2 and 3: Collisional Energy Transfer and the Master Equation 2019, 43, 465–514.
- (20) Barker, J. R. Monte Carlo stochastic simulation of the master equation for unimolecular reaction systems. *Unimolecular Kinetics:* Parts 2 and 3: Collisional Energy Transfer and the Master Equation **2019**, 43, 409–463.
- (21) Robertson, S. H. Foundations of the master equation. Unimolecular Kinetics: Parts 2 and 3: Collisional Energy Transfer and the Master Equation 2019, 43, 299–361.
- (22) Smith, S. C.; Frankcombe, T. J. Numerical methods. Unimolecular Kinetics: Parts 2 and 3: Collisional Energy Transfer and the Master Equation 2019, 43, 363–408.
- (23) Mokrushin, V.; Bedanov, V.; Tsang, W.; Zachariah, M. R.; Knyazev, V. D.; McGivern, W. S. ChemRate: A Tool for RRKM/Master Equation Modeling. V. 1.5.10, April 14, 2011.
- (24) Gilbert, R. G.; Jordan, M. J. T.; Smith, S. C. UNIMOL Program Suite; Sydney, Australia. 1993.
- (25) Glowacki, D. R.; Liang, C. H.; Morley, C.; Pilling, M. J.; Robertson, S. H. MESMER: an open-source master equation solver for multi-energy well reactions. *J. Phys. Chem. A* **2012**, *116* (38), 9545–60.
- (26) Robertson, S. H.; Glowacki, D. R.; Morley, C.; Liang, C. H.; Shannon, R. J.; Blitz, M.; Seakins, P.; Pilling, M. J.; Harvey, J. N. MESMER (Master Equation Solver for Multi Energy-well Reactions): An open source, general purpose program for calculating rate coefficients through solving the chemical master equation; University of Leeds: 2018.
- (27) Georgievskii, Y.; Klippenstein, S. J. MESS; Argonne National Laboratory: 2016.
- (28) Barker, J. R.; Nguyen, T. L.; Stanton, J. F.; Aieta, C.; Ceotto, M.; Gabas, F.; Kumar, T. J. D.; Li, C. G. L.; Lohr, L. L. et al. MULTIWELL Program Suite, Climate and Space Sciences and Engineering; University of Michigan: Ann Arbor, MI, 2017.
- (29) Le, T. N.-M.; Liu, B.; Huynh, L. K. SurfKin: An *ab initio* kinetic code for modeling surface reaction. *J. Comput. Chem.* **2014**, *35*, 1890–1899.

- (30) Nguyen, T. L.; Stanton, J. F. A Steady-State Approximation to the Two-Dimensional Master Equation for Chemical Kinetics Calculations. *J. Phys. Chem. A* **2015**, *119* (28), 7627–7636.
- (31) Nguyen, T. L.; Lee, H.; Matthews, D. A.; McCarthy, M. C.; Stanton, J. F. Stabilization of the Simplest Criegee Intermediate from the Reaction between Ozone and Ethylene: A High-Level Quantum Chemical and Kinetic Analysis of Ozonolysis. *J. Phys. Chem. A* **2015**, 119 (22), 5524–5533.
- (32) Nguyen, T. L.; McCaslin, L.; McCarthy, M. C.; Stanton, J. F. Communication: Thermal unimolecular decomposition of syn-CH<sub>2</sub>CHOO: A kinetic study. *J. Chem. Phys.* **2016**, *145* (13), 131102.
- (33) Nguyen, T. L.; Thorpe, J. H.; Bross, D. H.; Ruscic, B.; Stanton, J. F. Unimolecular Reaction of Methyl Isocyanide to Acetonitrile: A High-Level Theoretical Study. *J. Phys. Chem. Lett.* **2018**, 9 (10), 2532–2538.
- (34) Nguyen, T. L.; Ruscic, B.; Stanton, J. F. A master equation simulation for the OH + CH<sub>3</sub>OH reaction. *J. Chem. Phys.* **2019**, *150* (8), 084105.
- (35) Jasper, A. W.; Pelzer, K. M.; Miller, J. A.; Kamarchik, E.; Harding, L. B.; Klippenstein, S. J. Predictive a priori pressure-dependent kinetics. *Science* **2014**, *346* (6214), 1212–1215.
- (36) Smith, S. C.; Gilbert, R. G. Angular-Momentum Conservation in Unimolecular and Recombination Reactions. *Int. J. Chem. Kinet.* **1988**, 20 (4), 307–329.
- (37) Smith, S. C.; Gilbert, R. G. Angular-Momentum Conservation in Multichannel Unimolecular Reactions. *Int. J. Chem. Kinet.* **1988**, *20* (12), 979–990.
- (38) Troe, J. Theory of Thermal Unimolecular Reactions at Low-Pressures 0.1. Solutions of Master Equation. *J. Chem. Phys.* **1977**, *66* (11), 4745–4757.
- (39) Troe, J. Specific Rate Constants K(E,J) for Unimolecular Bond Fissions. J. Chem. Phys. 1983, 79 (12), 6017–6029.
- (40) Troe, J. The Polanyi Lecture the Colorful World of Complex-Forming Bimolecular Reactions. *J. Chem. Soc., Faraday Trans.* **1994**, 90 (16), 2303–2317.
- (41) Miller, W. H. Unified Statistical-Model for Complex and Direct Reaction-Mechanisms. *J. Chem. Phys.* **1976**, 65 (6), 2216–2223.
- (42) Miller, W. H. Tunneling Corrections to Unimolecular Rate Constants, with Application to Formaldehyde. *J. Am. Chem. Soc.* **1979**, *101* (23), *6810–6814*.
- (43) Aubanel, E. E.; Wardlaw, D. M.; Zhu, L.; Hase, W. L. Role of Angular-Momentum in Statistical Unimolecular Rate Theory. *Int. Rev. Phys. Chem.* **1991**, *10* (3), 249–286.
- (44) Zhu, L.; Hase, W. L. Comparison of Models for Calculating the Rrkm Unimolecular Rate Constant-K(E,J). *Chem. Phys. Lett.* **1990**, 175 (1–2), 117–124.
- (45) Zhu, L.; Chen, W.; Hase, W. L.; Kaiser, E. W. Comparison of Models for Treating Angular-Momentum in Rrkm Calculations with Vibrator Transition-States Pressure and Temperature-Dependence of Cl+C<sub>2</sub>H<sub>2</sub> Association. *J. Phys. Chem.* **1993**, *97* (2), 311–322.
- (46) Jeffrey, S. J.; Gates, K. E.; Smith, S. C. Full Iterative Solution of the Two-Dimensional Master Equation for Thermal Unimolecular Reactions. *J. Phys. Chem.* **1996**, *100*, 7090–7096.
- (47) Robertson, S. H.; Pilling, M. J.; Gates, K. E.; Smith, S. C. Application of inverse iteration to 2-dimensional master equations. *J. Comput. Chem.* **1997**, *18* (8), 1004–1010.
- (48) Venkatesh, P. K.; Dean, A. M.; Cohen, M. H.; Carr, R. W. Master equation analysis of intermolecular energy transfer in multiple-well, multiple-channel unimolecular reactions. II. Numerical methods and application to the mechanism of the C<sub>2</sub>H<sub>5</sub>+O<sub>2</sub> reaction. *J. Chem. Phys.* **1999**, *111* (18), 8313–8329.
- (49) Barker, J. R.; Weston, R. E. Collisional Energy Transfer Probability Densities P(E, J; E ' J ') for Monatomics Colliding with Large Molecules. *J. Phys. Chem. A* **2010**, *114* (39), 10619–10633.
- (50) Barker, J. R.; Weston, R. E. Collisional Energy Transfer Probability Densities P(E,J;E ',J ') for Monatomics Colliding with Large Molecules (vol 114, 10619, 2010). *J. Phys. Chem. A* **2012**, *116* (1), 799–799a.

- (51) Robertson, S. H. Parametric models. *Unimolecular Kinetics:* Parts 2 and 3: Collisional Energy Transfer and the Master Equation **2019**, 43, 273–295.
- (52) King, K. D.; Barker, J. R. Experiments on collisional energy transfer. *Unimolecular Kinetics: Parts 2 and 3: Collisional Energy Transfer and the Master Equation* **2019**, 43, 3–62.
- (53) Tardy, D. C.; Rabinovitch, B. S. Intermolecular Vibrational Energy-Transfer in Thermal Unimolecular Systems. *Chem. Rev.* **1977**, 77 (3), 369–408.
- (54) Oref, I.; Rabinovitch, B. S. Vibrational-Translational Energy-Transfer in Atom-Polyatomic Molecule Collisions in Thermal-Reaction Systems. *Chem. Phys.* **1977**, *26* (3), 385–392.
- (55) Jasper, A. W.; Miller, J. A. Theoretical Unimolecular Kinetics for  $CH_4+M$  reversible arrow  $CH_3+H+M$  in Eight Baths, M=He, Ne, Ar, Kr,  $H_2$ ,  $N_2$ , CO, and  $CH_4$ . J. Phys. Chem. A **2011**, 115 (24), 6438–6455.
- (56) Reid, R. C.; Prausnitz, J. M.; Sherwood, T. K. The Properties of Gases and Liquids; 1977.
- (57) Lendvay, G. Classical trajectory studies of collisional energy transfer. *Unimolecular Kinetics: Parts 2 and 3: Collisional Energy Transfer and the Master Equation* **2019**, 43, 109–272.
- (58) Lendvay, G.; Schatz, G. C. Quantum scattering theory for collisional energy transfer. *Unimolecular Kinetics: Parts 2 and 3: Collisional Energy Transfer and the Master Equation* **2019**, 43, 63–107.
- (59) Hippler, H.; Troe, J.; Wendelken, H. J. Collisional Deactivation of Vibrationally Highly Excited Polyatomic-Molecules 0.3. Direct Observations for Substituted Cycloheptatrienes. *J. Chem. Phys.* **1983**, 78 (11), 6718–6724.
- (60) Troe, J. Theory of Thermal Unimolecular Reactions at Low-Pressures 0.2. Strong Collision Rate Constants Applications. *J. Chem. Phys.* **1977**, *66* (11), 4758–4775.
- (61) Klippenstein, S. J.; Wagner, A. F.; Robertson, S. H.; Dunbar, R.; Wardlaw, D. *VARIFLEX*; Chemistry Division, Argonne National Laboratory: 1999.
- (62) Bartis, J. T.; Widom, B. Stochastic models of the interconversion of three or more chemical species. *J. Chem. Phys.* **1974**, *60*, 3474–3482.
- (63) Lehoucq, R. B.; Sorensen, D. C.; Yang, C.; Society for Industrial and Applied Mathematics., ARPACK users' guide solution of large-scale eigenvalue problems with implicitly restarted Arnoldi methods. In *Software, environments, tools* 6. [Online] Society for Industrial and Applied Mathematics: Philadelphia, PA, 1998; http://epubs.siam.org/ebooks/siam/software\_environments\_and\_tools/se06
- (64) Anderson, E.; Bai, Z.; Bischof, C.; Blackford, S.; Demmel, J.; Dongarra, J.; Du Croz, J.; Greenbaum, A.; Hammarling, S. et al. *LAPACK*; Society for Industrial and Applied Mathematics: 1999.
- (65) Hanninglee, M. A.; Green, N. J. B.; Pilling, M. J.; Robertson, S. H. Direct Observation of Equilibration in the System  $H+C_2H_4 \leftrightarrow C_2H_5$  Standard Enthalpy of Formation of the Ethyl Radical. *J. Phys. Chem.* **1993**, 97 (4), 860–870.
- (66) Green, N. J. B.; Marchant, P. J.; Perona, M. J.; Pilling, M. J.; Robertson, S. H. Forward and Reverse Rate Coefficients in Equilibrating Isomerization-Reactions. *J. Chem. Phys.* **1992**, *96* (8), 5896–5907.
- (67) Schneider, F. W.; Rabinovitch, B. S. Thermal Unimolecular Isomerization of Methyl Isocyanide Fall-Off Behavior. *J. Am. Chem. Soc.* **1962**, *84* (22), 4215–4230.
- (68) Fletcher, F. J.; Rabinovitch, B. S.; Watkins, K. W.; Locker, D. J. Energy Transfer in Thermal Methyl Isocyanide Isomerization. Experimental Survey. *J. Phys. Chem.* **1966**, *70* (9), 2823–2833.
- (69) Rabinovitch, B. S.; Lin, Y. N.; Chan, S. C.; Watkins, K. W. Energy Transfer in Thermal Methyl Isocyanide Isomerization. Collison Cross Sections of N-Alkanes. *J. Phys. Chem.* **1967**, *71* (11), 3715–3716.
- (70) Collister, J. L.; Pritchard, H. O. Thermal-Isomerization of Methyl Isocyanide in Temperature-Range 120–320degreesc. *Can. J. Chem.* **1976**, *54* (15), 2380–2384.

- (71) Wang, D. X.; Qian, X. M.; Peng, J. A novel method for the kinetic study of a chemical reaction. Determination of the kinetic parameters of the isomerisation reaction of methyl isocyanide using HeI photoelectron spectroscopy. *Chem. Phys. Lett.* **1996**, 258 (1–2), 149–154.
- (72) Harris, H. H.; Bunker, D. L. Methyl Isocyanide Is Probably a Non-Rrkm Molecule. *Chem. Phys. Lett.* **1971**, *11* (4), 433–436.
- (73) Bunker, D. L.; Hase, W. L. Non-Rrkm Unimolecular Kinetics Molecules in General, and Ch3nc in Particular. *J. Chem. Phys.* **1973**, 59 (9), 4621–4632.
- (74) Jayee, B.; Malpathak, S.; Ma, X.; Hase, W. L. Is CH<sub>3</sub>NC isomerization an intrinsic non-RRKM unimolecular reaction? *J. Chem. Phys.* **2019**, *151* (18), 184110.
- (75) Miller, J. A.; Bowman, C. T. Mechanism and Modeling of Nitrogen Chemistry in Combustion. *Prog. Energy Combust. Sci.* **1989**, 15 (4), 287–338.
- (76) Hinokuma, S.; Kiritoshi, S.; Kawabata, Y.; Araki, K.; Matsuki, S.; Sato, T.; Machida, M. Catalytic ammonia combustion properties and operando characterization of copper oxides supported on aluminum silicates and silicon oxides. *J. Catal.* **2018**, *361*, 267–277.
- (77) Kang, D. W.; Holbrook, J. H. Use of NH<sub>3</sub> fuel to achieve deep greenhouse gas reductions from US transportation. *Energy Rep* **2015**, 1, 164–168.
- (78) Boretti, A. A. Novel heavy duty engine concept for operation dual fuel H<sub>2</sub>-NH<sub>3</sub>. *Int. J. Hydrogen Energy* **2012**, *37* (9), 7869–7876. (79) *NH*<sub>3</sub> *Fuel Association: The Key to Energy Independence*; https://nh3fuelassociation.org/tag/fuel-economy/.
- (80) Nguyen, T. L.; Stanton, J. F. Three-Dimensional Master Equation (3DME) Approach. J. Phys. Chem. A 2018, 122 (38), 7757–7767.
- (81) Criegee, R. Mechanism of Ozonolysis. *Angew. Chem., Int. Ed. Engl.* **1975**, *14* (11), 745–752.
- (82) Criegee, R. An oxidative fission of glycols (II. Communication. On oxidations with lead(IV)-salts)). *Ber. Dtsch. Chem. Ges. B* **1931**, 64, 260–266.
- (83) Taatjes, C. A.; Meloni, G.; Selby, T. M.; Trevitt, A. J.; Osborn, D. L.; Percival, C. J.; Shallcross, D. E. Direct observation of the gasphase Criegee intermediate (CH<sub>2</sub>OO). *J. Am. Chem. Soc.* **2008**, *130* (36), 11883–5.
- (84) Osborn, D. L.; Taatjes, C. A. The physical chemistry of Criegee intermediates in the gas phase. *Int. Rev. Phys. Chem.* **2015**, 34 (3), 309–360
- (85) Womack, C. C.; Martin-Drumel, M. A.; Brown, G. G.; Field, R. W.; McCarthy, M. C. Observation of the simplest Criegee intermediate CH<sub>2</sub>OO in the gas-phase ozonolysis of ethylene. *Sci. Adv.* **2015**, *1* (2), No. e1400105.
- (86) Nakajima, M.; Endo, Y. Communication: Determination of the molecular structure of the simplest Criegee intermediate CH<sub>2</sub>OO. *J. Chem. Phys.* **2013**, *139* (10), 101103.
- (87) Su, Y. T.; Huang, Y. H.; Witek, H. A.; Lee, Y. P. Infrared absorption spectrum of the simplest Criegee intermediate CH<sub>2</sub>OO. *Science* **2013**, 340 (6129), 174–6.
- (88) Buras, Z. J.; Elsamra, R. M.; Green, W. H. Direct Determination of the Simplest Criegee Intermediate ( $CH_2OO$ ) Self Reaction Rate. *J. Phys. Chem. Lett.* **2014**, 5 (13), 2224–8.
- (89) Lee, Y. P. Perspective: Spectroscopy and kinetics of small gaseous Criegee intermediates. *J. Chem. Phys.* **2015**, *143* (2), 020901.
- (90) Atkinson, R. Gas-Phase Tropospheric Chemistry of Volatile Organic Compounds: 1. Alkanes and Alkenes. *J. Phys. Chem. Ref. Data* 1997, 26, 215–290.
- (91) Novelli, A.; Vereecken, L.; Lelieveld, J.; Harder, H. Direct observation of OH formation from stabilised Criegee intermediates. *Phys. Chem. Phys.* **2014**, *16* (37), 19941–51.
- (92) Taatjes, C. A.; Shallcross, D. E.; Percival, C. J. Research frontiers in the chemistry of Criegee intermediates and tropospheric ozonolysis. *Phys. Chem. Chem. Phys.* **2014**, *16* (5), 1704–18.
- (93) Fang, Y.; Liu, F.; Barber, V. P.; Klippenstein, S. J.; McCoy, A. B.; Lester, M. I. Communication: Real time observation of

unimolecular decay of Criegee intermediates to OH radical products. *J. Chem. Phys.* **2016**, *144* (6), 061102. (94) Long, B.; Bao, J. L.; Truhlar, D. G. Atmospheric Chemistry of

- (94) Long, B.; Bao, J. L.; Truhlar, D. G. Atmospheric Chemistry of Criegee Intermediates: Unimolecular Reactions and Reactions with Water. J. Am. Chem. Soc. **2016**, 138 (43), 14409–14422.
- (95) Long, B.; Bao, J. L.; Truhlar, D. G. Rapid unimolecular reaction of stabilized Criegee intermediates and implications for atmospheric chemistry. *Nat. Commun.* **2019**, *10*, 2003.